nature portfolio

https://doi.org/10.1038/s41596-021-00670-7

Supplementary information

Bioconjugates of photon-upconversion nanoparticles for cancer biomarker detection and imaging

In the format provided by the authors and unedited

nature portfolio

https://doi.org/10.1038/s41596-021-00670-7

Supplementary information

Bioconjugates of photon-upconversion nanoparticles for cancer biomarker detection and imaging

In the format provided by the authors and unedited

- Supplementary Information -

Bioconjugates of photon-upconversion nanoparticles for cancer biomarker detection and imaging

Antonín Hlaváček*[1], Zdeněk Farka*[2,3], Matthias J. Mickert[4], Uliana Kostiv[5], Julian C. Brandmeier[2,6], Daniel Horák[5], Petr Skládal[2,3], František Foret[1], Hans H. Gorris*[2]

[1]Institute of Analytical Chemistry of the Czech Academy of Sciences, Veveří 97, 602 00 Brno, Czech Republic

[2]Department of Biochemistry, Faculty of Science, Masaryk University, Kamenice 5, 625 00 Brno, Czech Republic

[3]CEITEC MU, Masaryk University, Kamenice 5, 625 00 Brno, Czech Republic

[4]Lumito AB, Mårtenstorget 5, 223 51, Lund, Sweden

[5]Institute of Macromolecular Chemistry of the Czech Academy of Sciences, Heyrovského nám. 2, 162 06 Prague 6, Czech Republic

[6]Institute of Analytical Chemistry, Chemo- and Biosensors, University of Regensburg, Universitätsstraße 31, 93040 Regensburg, Germany

Supplementary Table 1 | Quantum yields ($\Phi = N_{\text{photons emitted}}/N_{\text{photons absorbed}}$) of UCNPs reported in the literature. In case of UCNPs, the emission of each photon requires the absorption of at least 2 photons. Therefore, Φ cannot exceed 50 % and Φ depends on the excitation intensity. At high excitation intensities, the upconversion luminescence reaches a saturation level such that the total number of emitted photons is a better parameter for characterizing the performance of UCNPs than Φ.

Type	Size	Excitation wavelength	Excitation intensity	Quantum yield (Φ)	Dispersion medium	Ref.
Low excitation intensity:						
α-$NaYb_{0.995}Tm_{0.005}F_4$@$CaF_2$	27 nm	980 nm	0.3 W cm^{-2}	0.6%	Hexane	1
β-$NaY_{0.747}Yb_{0.25}Tm_{0.003}F_4$	33 nm	975 nm	3.8 W cm^{-2}	0.45%	Hexane	2
β-$NaY_{0.747}Yb_{0.25}Tm_{0.003}F_4$@$NaYF_4$	43 nm		1.3 W cm^{-2}	1.2%		
β-$NaY_{0.68}Yb_{0.30}Er_{0.02}F_4$@ $NaY_{0.80}Yb_{0.20}F_4$@$NaY_{0.90}Yb_{0.10}F_4$	40 nm	980 nm	2.0 W cm^{-2}	0.22%	Cyclohexane	3
α-$NaY_{0.90}Er_{0.10}F_4$ @$NaYbF_4$@$NaYF_4$	32 nm	980 nm	4.5 W cm^{-2}	6.3%	Cyclohexane	4
$LiY_{0.745}Yb_{0.25}Tm_{0.005}F_4$	87×50 nm	976 nm	5.5 W cm^{-2}	1.9%	Toluene	5
Medium excitation intensity:						
β-$NaY_{0.747}Yb_{0.25}Tm_{0.003}F_4$@$NaYF_4$	42 nm	975 nm	78 W cm^{-2}	3.5%	Hexane	6
β-$NaY_{0.798}Yb_{0.20}Tm_{0.002}F_4$	30 nm	980 nm	140 W cm^{-2}	0.8%	Toluene	7
β-$NaY_{0.795}Yb_{0.20}Tm_{0.005}F_4$				3.1%		
β-$NaY_{0.792}Yb_{0.20}Tm_{0.008}F_4$				5.4%		
β-$NaY_{0.788}Yb_{0.20}Tm_{0.012}F_4$				8.4%		
β-$NaY_{0.780}Yb_{0.20}Tm_{0.02}F_4$				3.6%		
$LiY_{0.745}Yb_{0.25}Tm_{0.005}F_4$	87×50 nm	976 nm	395 W cm^{-2}	3.3%	Toluene	5
β-$NaY_{0.78}Yb_{0.20}Er_{0.02}F_4$	>>100 nm	980 nm	20 W cm^{-2}	3.0%	No dispersion medium	8
β-$NaYb_{0.69}Er_{0.30}Tm_{0.01}$@$NaLuF_4$	28 nm	980 nm	10 W cm^{-2}	1.8%	Cyclohexane	9
β-$NaErF_4$@$NaLuF_4$	35-38 nm	980 nm	10 W cm^{-2}	5.2%	Toluene	10
α-$NaEr_{0.02}Yb_{0.98}F_4$@CaF_2	14 nm	980 nm	34 W cm^{-2}	1%	Cyclohexane	11
β-$NaY_{0.78}Yb_{0.20}Er_{0.02}F_4$@$NaYF_4$	15 nm	976 nm	40 W cm^{-2}	3.4%		12
	45 nm			9.0%		
β-$NaYbF_4$@$NaY_{0.60}Er_{0.20}Gd_{0.20}F_4$@$NaY_{0.80}Gd_{0.20}F_4$	16 nm	980 nm	70 W cm^{-2}	0.02%	Hexane	13
β-$NaY_{0.58}Gd_{0.20}Yb_{0.20}Er_{0.02}F_4$@$NaY_{0.80}Gd_{0.20}F_4$				0.8%		
β-$NaY_{0.78}Yb_{0.20}Er_{0.02}F_4$	8 nm	976 nm	100 W cm^{-2}	0.011%	Hexane	14
β-$NaY_{0.78}Yb_{0.20}Er_{0.02}F_4$@$NaYF_4$	14 nm			0.49%		
$LiLu_{0.79}Yb_{0.20}Er_{0.01}F_4$	28 nm	980 nm	127 W cm^{-2}	0.11%	Cyclohexane	15
$LiLu_{0.79}Yb_{0.20}Er_{0.01}F_4$@$LiLuF_4$	40 nm			3.6%		
$LiLu_{0.79}Yb_{0.20}Er_{0.01}F_4$@$LiLuF_4$	50 nm			5.0%		
β-$NaY_{0.78}Yb_{0.20}Er_{0.02}F_4$	100 nm	980 nm	150 W cm^{-2}	0.30%	Hexane	8
β-$NaY_{0.78}Yb_{0.20}Er_{0.02}F_4$	30 nm			0.10%		
β-$NaY_{0.78}Yb_{0.20}Er_{0.02}F_4$	8-10 nm			0.005%		
β-$NaY_{0.78}Yb_{0.20}Er_{0.02}F_4$	30 nm			0.30%		
β-$NaY_{0.86}Yb_{0.11}Er_{0.03}F_4$	33.4 nm	976 nm	380 W cm^{-2}	2.50%	Toluene	16
β-$NaY_{0.83}Yb_{0.14}Er_{0.03}F_4$	34.0 nm		380 W cm^{-2}	2.30%		
β-$NaY_{0.80}Yb_{0.17}Er_{0.03}F_4$	33.8 nm		380 W cm^{-2}	1.96%		
β-$NaY_{0.76}Yb_{0.21}Er_{0.03}F_4$	34.2 nm		380 W cm^{-2}	1.73%		

β-$NaY_{0.85}Yb_{0.14}Er_{0.01}F_4$	33.6 nm		380 W cm^{-2}	2.52%		
β-$NaY_{0.84}Yb_{0.14}Er_{0.02}F_4$	32.9 nm		380 W cm^{-2}	2.13%		
β-$NaY_{0.82}Yb_{0.14}Er_{0.04}F_4$	32.8 nm		380 W cm^{-2}	1.75%		
β-$NaY_{0.80}Yb_{0.17}Er_{0.03}F_4$	32 nm		410 W cm^{-2}	1.4%	Toluene	[17]
β-$NaY_{0.78}Yb_{0.20}Er_{0.02}F_4$	23 nm	976 nm	~950 W cm^{-2}	~1%	Cyclohexane	[18]
			~950 W cm^{-2}	~1%	DMF	
			~800 W cm^{-2}	~0.5%	H_2O	
			~850 W cm^{-2}	~1%	D_2O	
β-$NaErF_4$@$NaYF_4$	20 nm	980 nm	?	0.17%	Cyclohexane	[19]
β-$NaEr_{0.995}F_4$:$Tm_{0.005}$@$NaYF_4$	29 nm	980 nm		0.78%		
β-$NaY_{0.80}Yb_{0.18}Er_{0.02}F_4$@$NaYF_4$	38 nm	980		1.83%		
(?) While not specified in the original work, the quantum yield reported for $NaY_{0.80}Yb_{0.18}Er_{0.02}F_4$@$NaYF_4$ indicates a medium excitation intensity.						
High excitation intensity:						
β-$NaY_{0.80-x}Yb_{0.20}Tm_xF_4$	40 nm	980 nm	2.5 × 10^6 W cm^{-2}	Not available	Cyclohexane	[20]
x = 0.002, 0.005, 0.01, 0.02, 0.04 and 0.08; $NaY_{0.72}Yb_{0.20}Tm_{0.08}F_4$ yielded the highest number of photons.						
β-$NaY_{0.78}Yb_{0.20}Er_{0.02}F_4$	8.0 nm	980 nm	3 × 10^6 W cm^{-2}	Not available		[14]
β-$NaY_{0.78}Yb_{0.02}Er_{0.20}F_4$	8.3 nm					
β-$NaY_{0.60}Yb_{0.20}Er_{0.20}F_4$	8.5 nm					
$NaY_{0.60}Yb_{0.20}Er_{0.20}F_4$ (8.5 nm) yielded the highest number of photons.						

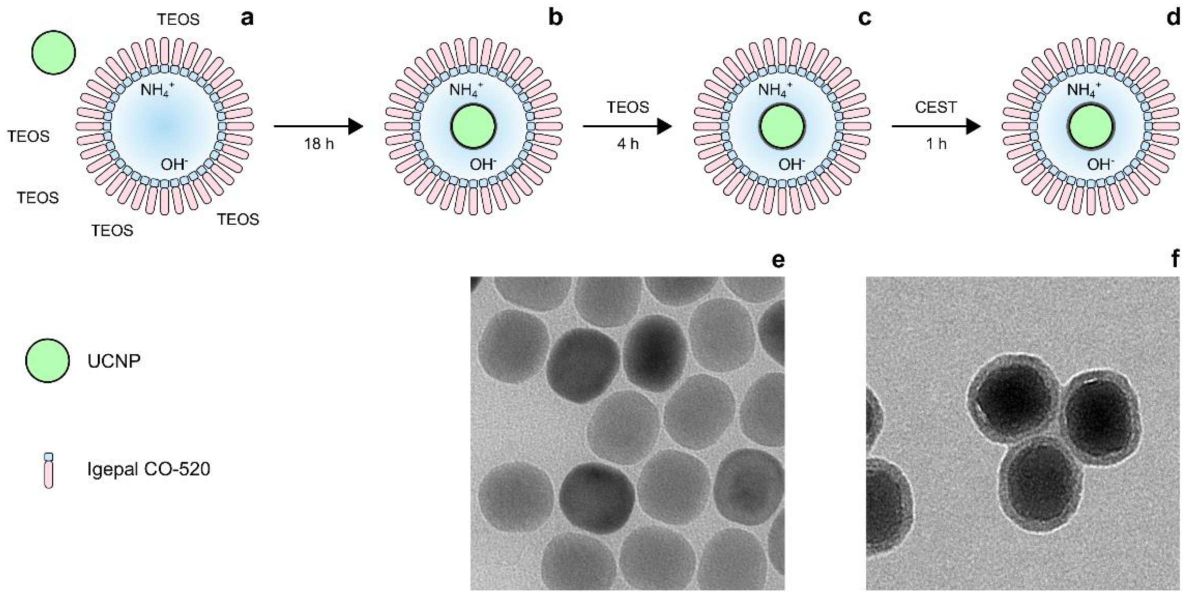

Supplementary Figure 1 | Preparation of UCNPs with a carboxylated silica shell via a reverse microemulsion technique. a, Dispersion of UCNPs in cyclohexane, TEOS, and Igepal CO-520-stabilized aqueous NH_4OH nanodroplets. **b**, Silica-coated UCNPs move to water droplets where the carboxylation takes place after adding (**c**) more TEOS and (**d**) CEST. TEM images of UCNPs ($NaYF_4$: 2%Er^{3+}, 18%Yb^{3+}, diameter 48.2±3.4 nm) covered by, **e**, oleic acid and, **f**, carboxylated silica shell (thickness 7.1±1.2 nm).

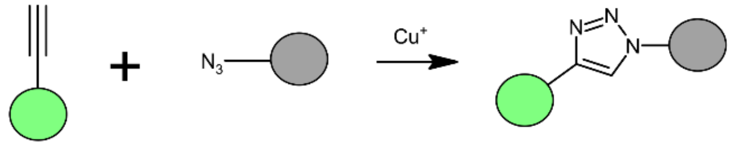

Supplementary Figure 2 | Bioconjugation via click-chemistry. Azide-modified biomolecules (gray circle) are bioconjugated to alkyne-PEG-neridronate-modified UCNPs (green circle) via a single copper-catalyzed reaction step.

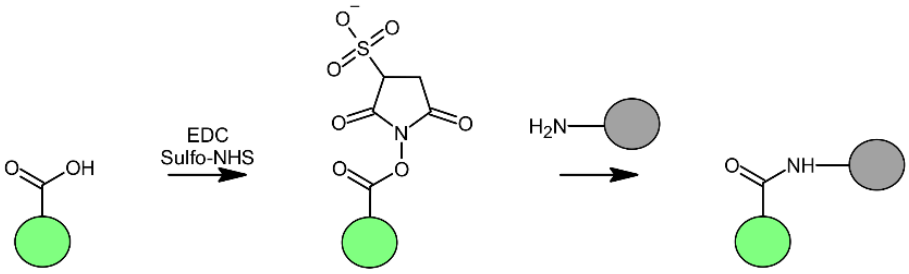

Supplementary Figure 3 | Bioconjugation via carbodiimide activation. Biomolecules containing primary amino groups (gray circle) are bioconjugated to carboxyl groups on the surface of UCNPs (green circle) in two steps. In the first step, the carboxyl groups are converted to esters in the presence of EDC and sulfo-NHS. Secondly, the activated UCNPs are conjugated to an amino group forming an amide bond.

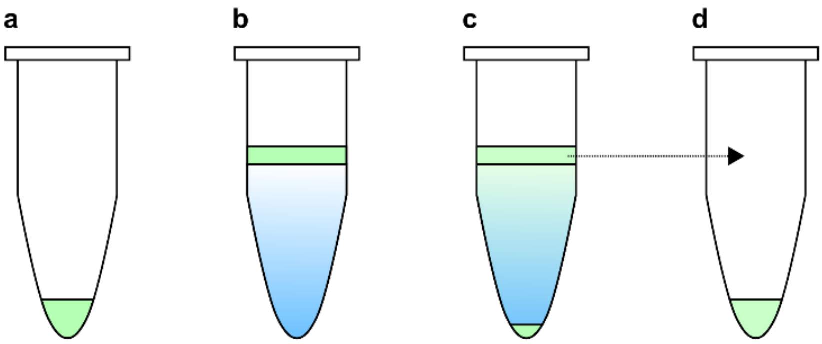

Supplementary Figure 4 | Centrifugal purification of bioconjugated UCNPs. a, Bioconjugated UCNPs (green) are placed into a centrifugal tube (1.5 mL). **b**, The sample is underlaid with a sucrose gradient (blue). **c**, After centrifugation, coarse aggregates remain at the bottom of the tube. **d**, The top layer containing purified bioconjugates is recovered and transferred to a new tube.

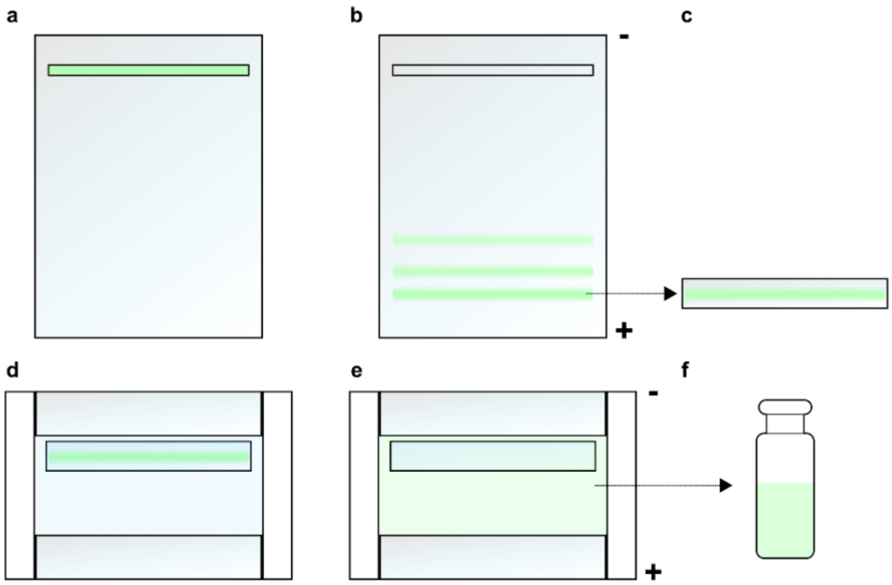

Supplementary Figure 5 | Electrophoretic purification of bioconjugated UCNPs. a, A sample of UCNP bioconjugate (green) is loaded into a wide gel pocket. **b**, After the application of an electric field, the sample constituents are fractionated according to their electrophoretic mobilities. **c**, The zone of interest is cut by a razor and isolated from the remaining gel. **d**, The gel slice containing the bioconjugate is inserted into the electro-elution chamber filled with electrophoresis buffer. **e**, The bioconjugated UCNPs are eluted into the buffer by applying an electric field. **f**, The eluted bioconjugate is transferred to a vial.

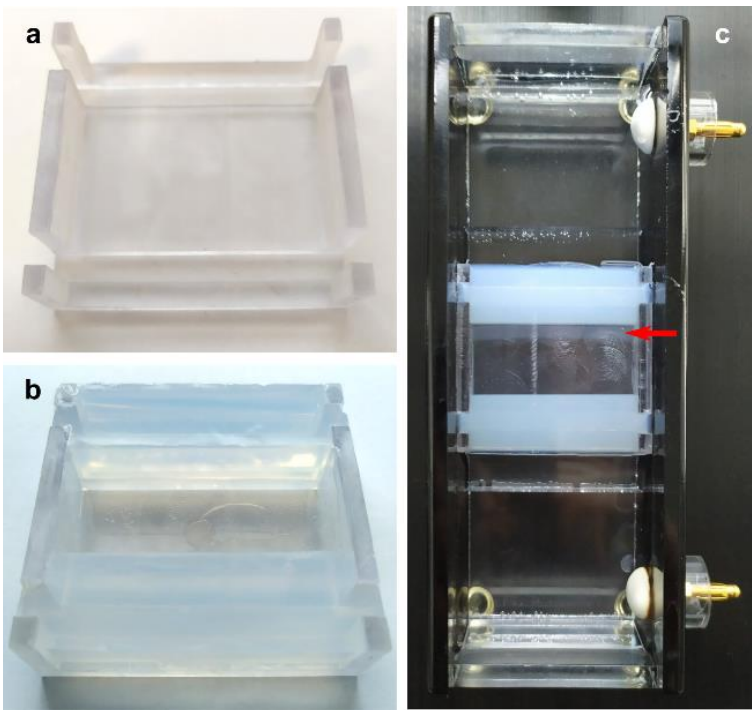

Supplementary Figure 6 | Images of electroelution chamber. The chamber is composed of a plastic frame (width 53 mm, length 50 mm) and two agarose gel slices, which create opposite walls of the chamber. **a**, Plastic frame before adding agarose walls. **b**, Chamber filled with agarose gel. **c**, Electroelution chamber inserted into the electrophoresis device. A gel slice containing a nanomaterial sample (red arrow) has been inserted into the chamber for electroelution.

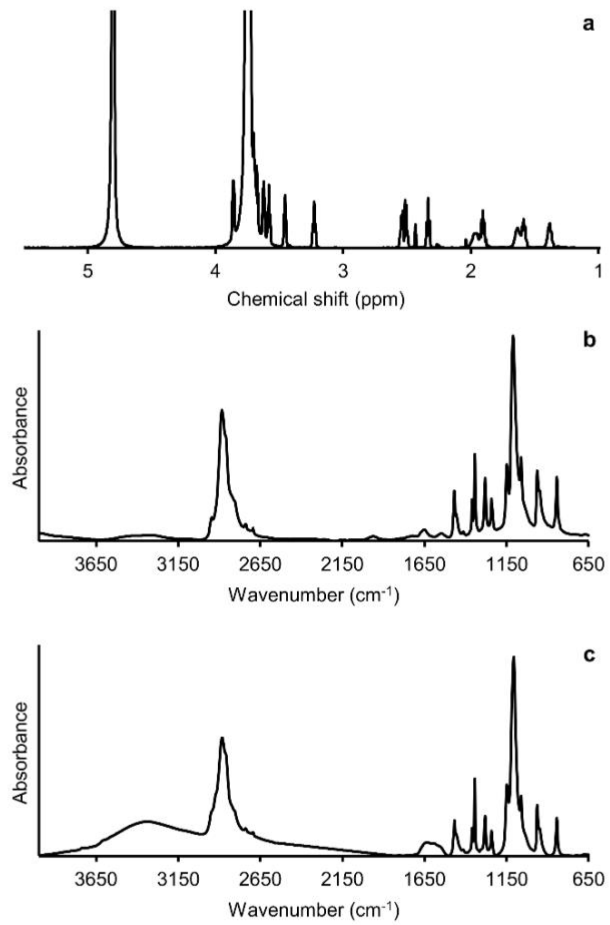

Supplementary Figure 7 | Spectroscopic characterization. a, ^{1}H NMR spectrum and **b**, ATR FTIR spectrum of alkyne-PEG-neridronate. **c**, ATR FTIR spectrum of alkyne-PEG-UCNPs.

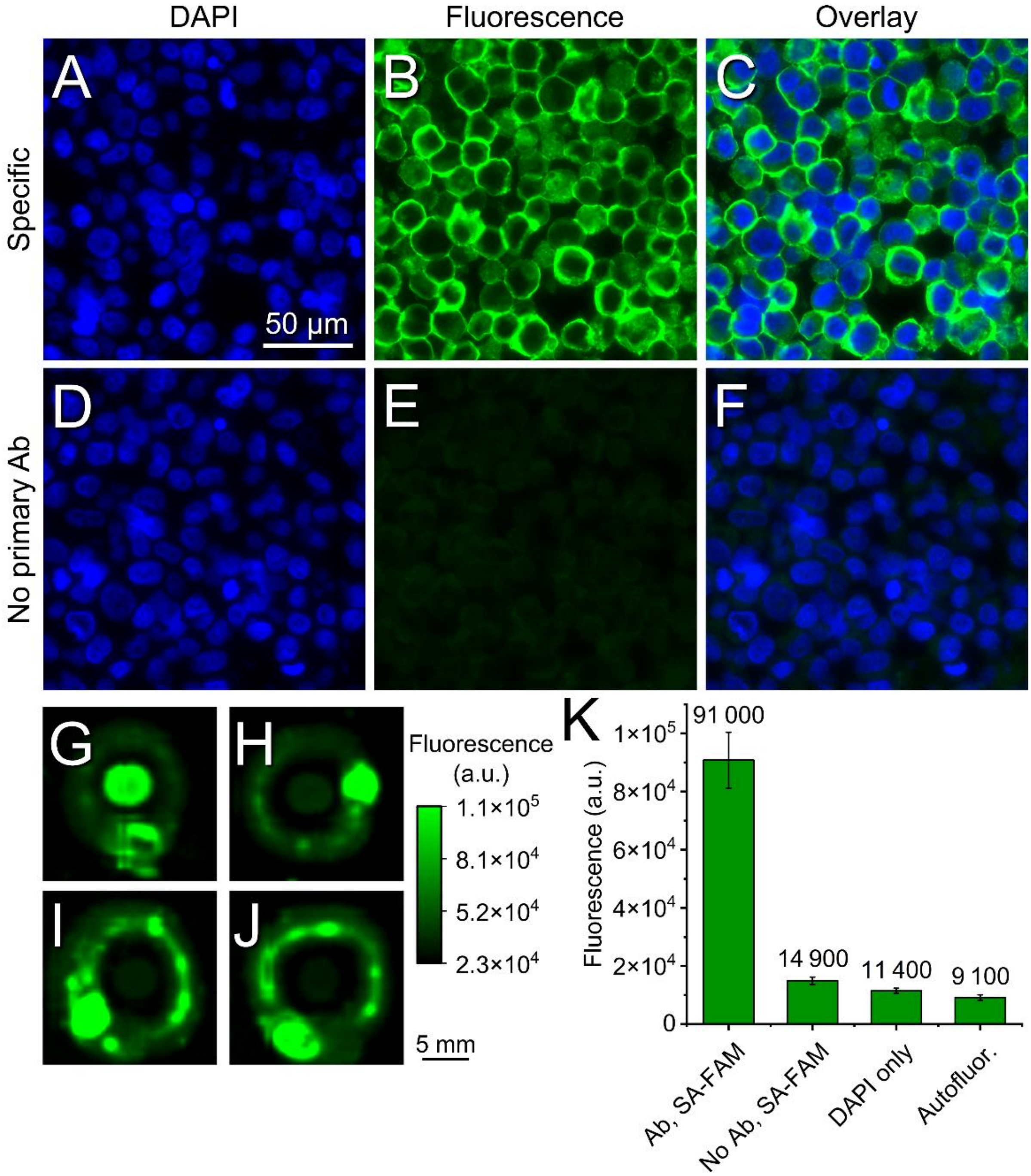

Supplementary Figure 8 | Fluorescence labeling of HER2-positive FFPE BT-474 cells with a streptavidin-5(6)-carboxyfluorescein conjugate. **a**, DAPI channel, **b**, fluorescein channel, **c**, overlay. Negative control without primary antibody (Ab): **d**, DAPI channel, **e**, fluorescein channel, **f**, overlay. Fluorescence intensity scans of **g**, specific labeling, **h**, negative control (no primary Ab), **i**, incubation with DAPI only, and **j**, autofluorescence. **k**, Average fluorescence intensities measured in the cell pellets. The error bars indicate standard deviations of intensities in the cell pellets. Reproduced from ref[21] with permission from the Royal Society of Chemistry.

References

1. Chen, G. *et al.* (α-$NaYbF_4:Tm^{3+}$)/CaF_2 Core/Shell Nanoparticles with Efficient Near-Infrared to Near-Infrared Upconversion for High-Contrast Deep Tissue Bioimaging. *ACS Nano* **6**, 8280–8287 (2012).
2. Liu, H. *et al.* Balancing power density based quantum yield characterization of upconverting nanoparticles for arbitrary excitation intensities. *Nanoscale* **5**, 4770–4775 (2013).
3. Zhong, Y., Rostami, I., Wang, Z., Dai, H. & Hu, Z. Energy Migration Engineering of Bright Rare-Earth Upconversion Nanoparticles for Excitation by Light-Emitting Diodes. *Adv. Mater.* **27**, 6418–6422 (2015).
4. Wang, J. *et al.* Enhancing multiphoton upconversion through energy clustering at sublattice level. *Nat. Mater.* **13**, 157–162 (2014).
5. Meijer, M. S. *et al.* Absolute upconversion quantum yields of blue-emitting $LiYF_4:Yb^{3+},Tm^{3+}$ upconverting nanoparticles. *Phys. Chem. Chem. Phys.* **20**, 22556–22562 (2018).
6. Xu, C. T. *et al.* High-Resolution Fluorescence Diffuse Optical Tomography Developed with Nonlinear Upconverting Nanoparticles. *ACS Nano* **6**, 4788–4795 (2012).
7. Kraft, M., Würth, C., Palo, E., Soukka, T. & Resch-Genger, U. Colour-optimized quantum yields of Yb, Tm Co-doped upconversion nanocrystals. *Methods Appl. Fluoresc.* **7**, 024001 (2019).
8. Boyer, J.-C. & Veggel, F. C. J. M. van. Absolute quantum yield measurements of colloidal $NaYF_4$: Er^{3+}, Yb^{3+} upconverting nanoparticles. *Nanoscale* **2**, 1417–1419 (2010).
9. Liu, J. *et al.* Low power density 980 nm-driven ultrabright red-emitting upconversion nanoparticles: Via synergetic Yb^{3+}/Tm^{3+} cascade-sensitization. *J. Mater. Chem. C* **7**, 13415–13424 (2019).
10. Johnson, N. J. J. *et al.* Direct Evidence for Coupled Surface and Concentration Quenching Dynamics in Lanthanide-Doped Nanocrystals. *J. Am. Chem. Soc.* **139**, 3275–3282 (2017).
11. Shen, B. *et al.* Revisiting the optimized doping ratio in core/shell nanostructured upconversion particles. *Nanoscale* **9**, 1964–1971 (2017).
12. Homann, C. *et al.* $NaYF_4$:Yb,Er/$NaYF_4$ Core/Shell Nanocrystals with High Upconversion Luminescence Quantum Yield. *Angew. Chem. Int. Ed.* **57**, 8765–8769 (2018).
13. Siefe, C. *et al.* Sub-20 nm Core-Shell-Shell Nanoparticles for Bright Upconversion and Enhanced Förster Resonant Energy Transfer. *J. Am. Chem. Soc.* **141**, 16997–17005 (2019).
14. Gargas, D. J. *et al.* Engineering bright sub-10-nm upconverting nanocrystals for single-molecule imaging. *Nat. Nanotechnol.* **9**, 300–305 (2014).
15. Huang, P. *et al.* Lanthanide-Doped $LiLuF_4$ Upconversion Nanoprobes for the Detection of Disease Biomarkers. *Angew. Chem. Int. Ed.* **53**, 1252–1257 (2014).
16. Kaiser, M., Würth, C., Kraft, M., Soukka, T. & Resch-Genger, U. Explaining the influence of dopant concentration and excitation power density on the luminescence and brightness of β-$NaYF_4:Yb^{3+},Er^{3+}$ nanoparticles: Measurements and simulations. *Nano Res.* **12**, 1871–1879 (2019).
17. Kaiser, M. *et al.* Power-dependent upconversion quantum yield of $NaYF_4:Yb^{3+},Er^{3+}$ nano- and micrometer-sized particles – measurements and simulations. *Nanoscale* **9**, 10051–10058 (2017).
18. Würth, C. *et al.* Excitation power dependent population pathways and absolute quantum yields of upconversion nanoparticles in different solvents. *Nanoscale* **9**, 4283–4294 (2017).
19. Chen, Q. *et al.* Confining Excitation Energy in Er^{3+}-Sensitized Upconversion Nanocrystals through Tm^{3+}-Mediated Transient Energy Trapping. *Angew. Chem. Int. Ed.* **56**, 7605–7609 (2017).
20. Zhao, J. *et al.* Single-nanocrystal sensitivity achieved by enhanced upconversion luminescence. *Nat. Nanotechnol.* **8**, 729–734 (2013).
21. Farka, Z. *et al.* Surface design of photon-upconversion nanoparticles for high-contrast immunocytochemistry. *Nanoscale* **12**, 8303–8313 (2020).